Discrete particle simulations and experiments on the collapse of wet granular columns

Fabio Gabrieli, Riccardo Artoni, Andrea Santomaso, Simonetta Cola

Discrete particle simulations and experiments on the collapse of wet granular columns

Fabio Gabrieli,[1, a)] Riccardo Artoni,[2] Andrea Santomaso,[3] and Simonetta Cola[1]
[1)] *Dept. of Civil, Environmental and Architectural Engineering (ICEA) University of Padova, via Ognissanti 39, 35129 Padova, Italy*
[2)] *L'UNAM, IFSTTAR, Route de Bouaye, CS4, 44344 Bouguenais Cedex, France*
[3)] *APTLab-Advanced Particle Technology Lab, Dept. of Industrial Engineering (DII) University of Padova, via Marzolo 9, 35131 Padova, Italy*

Small quantities of liquid in a granular material control the flow dynamics as well as the triggering and jamming phases. In order to study this problem some experimental collapse tests conducted in a rectangular box were reproduced with a 1:1 scale numerical model using the Discrete Element Method (DEM). In simulations the effect of the capillary bridges has been investigated implementing a mid-range attractive force between particles based on the minimum energy approach. Also a bonding-debonding mechanism was incorporated in the algorithm and the volume of each sessile drop on the particle surface was considered during its motion. The influence of some variables was investigated with respect to the final slope profiles and the runout lengths: the initial liquid content, the particle size, the solid density, the liquid surface tension and the liquid-solid contact angle. Also the crucial effect of the confinement walls on the collapse phenomenon was investigated: wet particles adhere to the lateral walls providing a higher flow resistance in comparison to the same material in dry conditions. It was observed that particles with largest path-lengths are localized near the movable wall at a middle-height of the initial column sample. Other particles at the surface moves in a rigid way especially if they were wet and with a low solid density. The "fidelity" of each particle with respect to the nearest neighbours was evaluated allowing to recognize the emergence of clusters of particles and rigid parts, to extract the failure surface and to localize where debonding mechanisms concentrate in the wet case.

PACS numbers: 45.70.Ht 47.57.Gc 83.80.Fg

I. INTRODUCTION

At least once in our lives we have played with sandcastles: experience has told us that in order to construct nearly vertical walls we needed to add a small amount of water to the material. Now we know that the stability of the sandcastles is due to the attractive forces between particles that arise only in partially saturated conditions.

In the last years this topic was studied by some authors[1–3] that realized the many existing links between the simple sandcastle and more complex civil engineering and geological problems like the assessment of the slope stability. A recent study[4] showed that the stability of cylindric sandcastles depends on the volumetric water content (in experiments with sand the authors found an optimum value of 1%) and on the aspect ratio (the maximum height is function of the base radius to the power of 2/3). They also reported the possibility to build underwater sandcastles using hydrophobic sand: in this case the "cohesive" properties of the partially saturated material were conserved by the presence of air menisci in place of water menisci.

Conventionally the saturation condition can be classified into five regimes[5] corresponding to five different physical conditions of the granular material. The dry state and the

[a)] Electronic mail: fabio.gabrieli@unipd.it

completely saturated conditions are the most known. The others are the pendular regime (when liquid is shared by pairs of grains), the funicular state (when liquid menisci coalesce grouping three or more particles) and the capillary state (when bubbles and menisci are present at the same time).

The completely saturated and the perfectly dry conditions (two-phase systems) share many similarities with respect to the mechanics of the granular material in static conditions. On the other hand, at intermediate conditions, the contemporary presence of liquid and air in the granular mass (three-phase systems) completely redefines the mechanical relationships between individual particles influencing the material behaviour at meso- and macro-scale.

At the contact scale, in static conditions, liquid-air interfaces are responsible of attractive (rarely repulsive, for convex menisci) forces between particles while lubrication, viscous and damping forces are reported in dynamic conditions[6,7]. At meso- and macro-scale some important secondary effects can be generally observed: a spontaneous agglomeration (granulation), an increase of the bulk density, a higher maximum packing density and an increase of the shear strength of the material. Many of these phenomena were studied at an "engineering scale", and usually the micromechanical interpretation is missing or unclear.

Also, the dynamic regime and the transitional phases (triggering and jamming) represent other important open issues that need to be addressed especially in the case of partially saturated conditions. The role of the liquid phase, the effect of the particle size and shape are only two of the several aspects that have important consequences in the landslide triggering in soil mechanics as well as in jamming/triggering problems in industrial processes such as handling, storage and transport. The results of the studies in this field can be the keystone to connect the classical solid mechanics (for quasi-static little deformations) with granular flow theories (for fully developed flows).

Collapse tests were considered as good reference tests in evaluating dynamic behaviour of liquids and granular materials in transient conditions[8] since they incorporate the triggering phase, the "fully-developed" flow and the final jammed state. Several authors studied the problem of the column collapse using dry granular materials[9–14], investigating the effect of the particle size and shape, the material type, the initial column geometry, and observing the shape of the final slope, the segregation, the kinematic of the front toe and other variables. Recently, other works focused on the collapse in fluids, which is the first step for the comprehension of the fully saturated granular flows, highlighting the effect of other variables which emerge in this case like the dilatancy behaviour linked with the initial volume fraction[15], and the opposing effect of viscous and lubrication forces[16]. Besides the laboratory tests many authors used particle numerical methods like the Discrete Element Method to model these experiments and to derive other useful contact-scale information[17–21].

The aim of these experiments and of the simulations was to collect information for the setting up of a continuum framework, in order to solve granular flow problems at an "engineering-scale". The original strategy was to use the depth-averaged shallow-water equations and to treat the material as a sort of viscous-frictional fluid[18,22–24]. However, as remarked by some authors[18,24,25], some difficulties arise using these approximations and other continuum approaches should be preferred to recognize the specificity of the spreading of the granular materials[26].

Our work wants to validate a particle-based model for the collapse tests of wet beads in pendular regime and to recognize the main micro and macromechanical variables that affect this problem.

We started from the study of the capillary force between two spheres, to provide a particle-scale model based on the Discrete Element Method taking into account liquid bridge failure, formation and redistribution. This model was used to reproduce and validate some collapse experiments at 1:1 scale with wet monosized glass spheres. After that some variables were modified in experiments and simulations: we focused on the use of different particle diameters, liquid amounts, surface tensions and boundary conditions. Other "virtual conditions", difficult to address in laboratory experiments, like the solid density of the particles and the liquid-air contact angle, were only simulated using the numerical model. The profiles provided by simulations were compared with the experiments from a qualitative and quan-

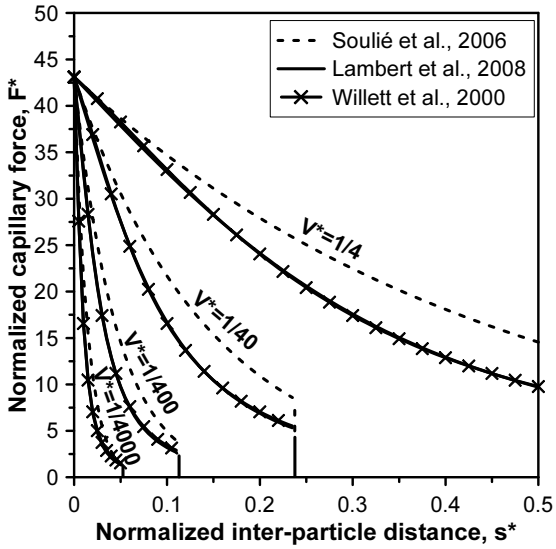

FIG. 1. Comparison of some capillary force models for a liquid bridge between two equal spheres ($D = 2$ mm, $\gamma = 72.75$ mN/m, $s^* = s/D$, $F^* = F_{cap}/(\rho g V_{sph})$, $V^* = V/V_{sph}$)

titative point of view, highlighting the critical aspects of the model assumptions; then, the particle dynamics was examined extracting useful information about the mechanisms of collapse for dry and wet initial conditions at different solid density.

II. THE CAPILLARY BRIDGE BETWEEN TWO EQUAL SPHERES

Let's consider a small liquid volume between two bodies. When the liquid surface tension and the solid-fluid adhesion prevents the fluid to flow away under the action of external forces (e.g. gravity), a pendular bridge is formed. At a microscale level, the meniscus is constrained to a finite set of possible shapes since its stability is controlled by an equilibrium between pressure in liquid phase and air pressure depending on the solid surface geometry and the physical interface properties.

There are at least two theories concerning the calculation of these shapes: the first is the classic Young-Laplace problem[27] that consists in solving a boundary value problem containing the expression of surface geometry of the menisci and the boundary conditions. The second concerns the solution of a minimum total energy problem that considers the energy of the system as the energy of the liquid volume added to the energy at each interface.

It can be proved that when two solid particles share a liquid phase the equilibrium of the system is not generally satisfied and attractive or repulsive forces emerge[28,29]. The interparticle force in a certain direction can be computed in two ways: as derivative of the total energy in that direction or decomposing all the forces in a section normal to that direction. Each of the two ways generally leads to a numerical solution[27,30,31]. Recently Lambert et al.[31] proved that the two approaches are equivalent for some simple geometrical shapes.

The most common solution of the menisci shape regards the liquid bridge between two equal spheres. Since generally no closed-form solution exists for this problem many other correlations were derived in the past. They can be classified in numerical and analytical/geometrical approximations[27,31,32], solutions derived from fitting of the latter[33,34] and solution derived from fitting of laboratory measures[35]. In Figure 1 a comparison of some selected normalized solutions is reported for the sphere-sphere case and for different capillary volumes.

Regardless of the solution adopted, qualitatively all the models describe the capillary

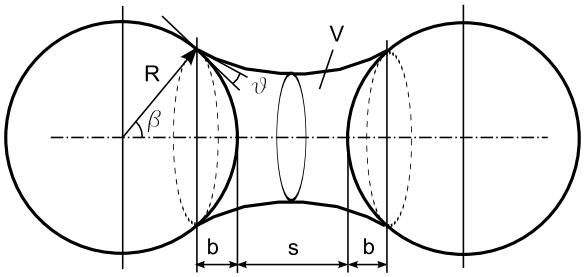

FIG. 2. Capillary bridge geometry.

force as a function of the capillary volume V, the gap s, the contact angle θ and the filling angle β (see Fig. 2). Pressure information (of air and/or liquid) should also be included especially if gas domain is not connected (it is not the case of the pendular state). In the following we will adopt the Lambert solution[31,36] that is simple, close to the laboratory data, suitable for integration into DEM and theoretically based at the same time.

All the models agree that the capillary attraction force has a maximum value ($2\pi R\gamma\cos\theta$) for gap, $s = 0$ (particles in contact) which is constant and independent of the liquid volume. This evidence was experimentally confirmed for a wide range of capillary volumes excepted for very small liquid volume where thermodynamic considerations and details about the surface roughness play a major role[37,38]. The force decreases with the distance up to a certain gap s_f at which the bridge breaks up. Lian et al.[27] observed that this critical distance is function of the liquid volume V and the contact angle θ:

$$s_f = \left(1 + \frac{\theta}{2}\right) V^{\frac{1}{3}} \tag{1}$$

On the other hand, the critical distance at which a given liquid volume can form a pendular bridge is[30]:

$$s_c = \frac{12V}{\pi\left(1 + \frac{1}{1-\cos\theta}\right)} \tag{2}$$

III. PENDULAR STATE DEM ALGORITHM

The algorithm used in reproducing the wet granular material behavior is the classical Discrete Element Method (DEM)[39] that integrates the motion of each particle starting from its initial position, imposing the external forces (like gravity) and computing contact forces derived from the constitutive model at the contacts. For dry conditions, the classical contact model consists in a linear spring with a viscous dashpot in normal direction and a linear spring plus a slider and a dashpot in tangential direction. DEM allows in a simple way the addition of variable custom forces thanks to the explicit nature of the algorithm which is based on the separation between the integration of the Newton's laws of motion and the computation of the forces at the contact. In our case, a liquid bridge model was implemented to study the material in the pendular regime.

The liquid bridge model is constituted of three parts: the first part manages the initial distribution of the liquid among contacts and particles and it is called at the initial steps.

The second part couples the classical DEM contact mechanics with the capillary force model. It treats the capillary attraction forces as mid-range forces in addition to the dry contact force mechanics that instead act only for overlapping particle. This part was treated in detail in Gabrieli et al.[36] considering specifically a two-particle system with different kinematic constraints.

The third part checks the formation of new capillary bridges from single or multiple drops and the failure of liquid bridges that reach the rupture distance (see Appendix B for the details). The total liquid volume was maintained constant during the simulations.

A. On the initial distribution of liquid

The liquid distribution in a granular material depends on many factors: the liquid amount, the initial solid packing density, the liquid properties and the "history" of the sample. As remarked by Scholtes et al.[40], the initial capillary bridge distribution has an important effect on the mechanical response of the material, therefore an initial distribution that mimics the initial real sample is desirable.

For this purpose, some micro-tomographic tests were performed on small cylindrical samples of glass spheres mixed with water. The observation of the reconstructed slices allowed to highlight that the initial distribution of liquid volume in the mass was homogeneous and well distributed on about the 96% of contacts[41]. No triple menisci could be recognized; this was verified for liquid contents typical of the pendular regime ($w < 4\%$).

In order to obtain a liquid content in the numerical sample consistent with the experimental observations, the following strategy was adopted: a) the couples of particles sustaining a liquid volume (called "potential contacts") were identified as those with a distance lower than s_f (from Eq. 1 this value in turn depends on the capillary volume); b) the total liquid volume was subdivided randomly among 96% of the potential contacts starting from a trial value of the capillary bridge volume and iteratively verifying the total amount of fluid, checking the critical distances and the homogeneity of the distribution. At the end of this procedure each capillary bond had the same liquid volume. Using this method, it was possible to find an initial stable particle configuration and the assembly was allowed to relax without any artificial localized tension.

B. The capillary force model

The capillary force model represents the heart of the pendular model. Let us consider two equal particles sharing a capillary bridge. Using the interface energy theory[28] it is possible to write down the analytical expression of the total energy of a bridge. Deriving this energy with respect to the gap between the particles, with some geometrical approximations, the attraction force exerted on two particles can be obtained. This finally depends on the capillary volume V and the gap s (see Appendix A for the details):

$$F_{cap}(s,V) = -\frac{2\pi R\gamma\cos\theta}{1+[s/2b(s,V)]} \tag{3a}$$

$$b(s,V) = (s/2)\left[-1+\sqrt{1+2V/(\pi R s^2)}\right] \tag{3b}$$

where γ is the liquid surface tension, θ the contact angle and b the wet spherical segment on sphere surface. Eq. 3a is valid for $s < s_f$; otherwise the bridge breaks up and no attractive force exists. With this assumption the capillary force model describes a mid-range interaction, with a cutoff at $s = s_f$. When particles are in contact, the attractive pendular force is added to the classical soft-sphere repulsive contact force; if not, only the capillary force (in addition to gravity) is considered for integrating the equation of motion. Because of their mid-range nature, the implementation of capillary forces involves an increase in the computational cost of the algorithm due to the enlargement of the Verlet cell of every particle.

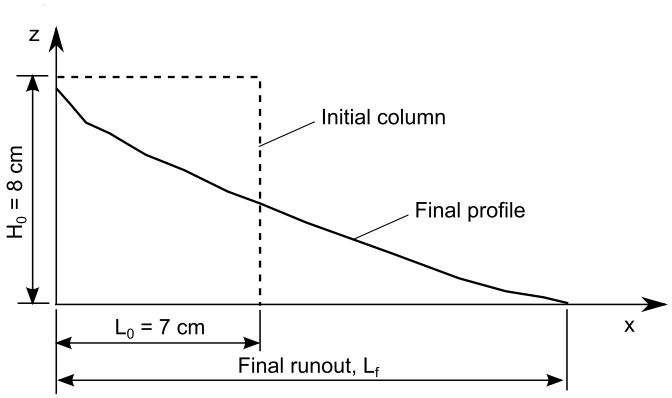

FIG. 3. Layout of a collapse test.

TABLE I. Measured liquid parameters

Liquid type	Surface tension[a] γ [mN/m]	Contact angle[b] θ [^{o}]
water	72.75	15
water + surfactant	17.1	40

[a] Measured with the ring method.
[b] Measured taking telecentric photos of a sessile drop on a flat surface cleaned with ethanol.

IV. COLUMN COLLAPSE EXPERIMENTS

Collapse experiments are quick laboratory tests, quite simple to perform and that require only the use of a camera. From the time-lapse images of the collapse, using digital image analysis techniques, "in-plane" quantities like velocity field or profiles of the slope can be easily measured.

Our experimental program consisted of several collapse tests performed within the same initial cuboid geometry (size 7 x 8 x 5 cm) in a transparent glass box (see Figure 3). The initial granular column was created by pouring the wet materials with a funnel in the fixed box. To start the test one of the glass lateral walls was lifted by a weight/pulley system. Each test was captured using a semi-professional high-resolution camera (Casio EX-F1) using a frame rate of 30 fps. The analysis of the image sequence enabled us to obtain the time evolution of the granular mass and to measure the profiles at each time step.

The sequence of images were analyzed to extract the surface slope of the material from the beginning of the collapse up to the final rest configuration of the pile. The mean final profile of a group of tests was obtained by averaging the z coordinates of the surfaces along the vertical axis. From the surface profiles, the slopes at different locations and the runout lengths L_f were extracted (see Fig. 3).

Mono-disperse glass spheres with different size (2, 3 and 5 mm in diameter D) were used in various wetting conditions (liquid contents w = 0, 0.5, 1, 2 and 4% of the weight of the dry materials). Two wetting liquids were used: distilled water and a mixture of water and a fluorinated surfactant (1-perfluorotooctyl-3-propan-2-ol with a concentration of 0.5 g/l) that allowed to decrease the surface tension. The physical parameters for the liquid phase (liquid surface tension γ and contact angle θ), were measured with dedicated laboratory tests and were reported in Table I.

Figure 4 shows two typical final configurations of the pile of material after the collapse in the dry and the wet cases. It is evident that the main effect of the capillary forces is to give a shorter run out and as a consequence a larger slope of the final profile. However in order to better understand the phenomenon a more detailed analysis is required.

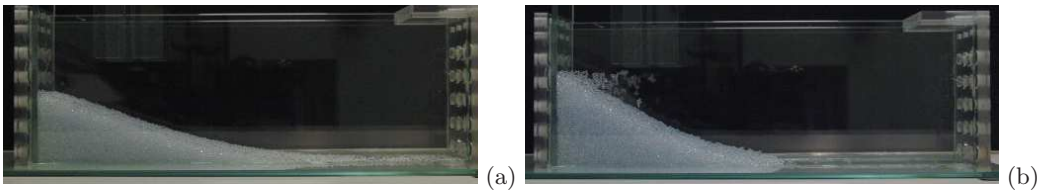

FIG. 4. Snapshots of the final profiles for $D = 2$ mm: (a) dry conditions; (b) wet conditions ($\gamma = 72.75$ mN/m; liquid content $w = 0.5\%$).

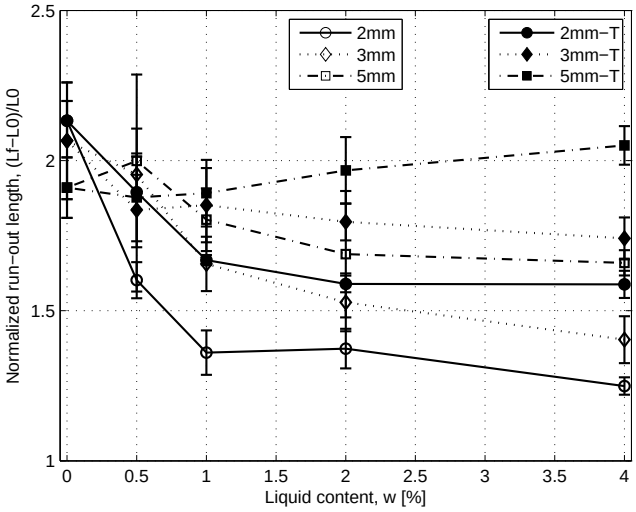

FIG. 5. Mean normalized runout lengths for all the experimental tests. The suffix T in the legend refers to the cases with water and surfactant

For the sake of shortness only some selected results will be presented here while further details can be found in Artoni et al.[42].

Figure 5 represents the mean normalized runout length obtained in all the experiments. Each group of tests with the same diameter was connected with a piece-wise line in order to facilitate the reading of the trends.

The first observation is that the collapse characteristics depended on both liquid content and particle size: the smallest particles ($D = 2$ mm) showed the strongest dependence on the moisture content while considering the coarser material (from $D = 3$ to 5 mm) the runout length decreased weakly with the moisture content (with exception of the case $w = 0.5\%$, $D = 5$ mm).

Furthermore, it should be noted that for the finest material the variation of runout length with liquid content was greater passing from dry to $w = 1\%$ and it reached a quite constant value for higher moisture content values ($w > 1\%$).

Lowering surface tension generally shifted the runout length values towards the dry results (with exception $D = 2$ and 3 mm, $w = 0.5\%$). Even for the coarsest material the "wet" runout lengths are slightly higher than the dry values; this effect could be attributed to the lubrication of the contacts that could arise in these conditions.

As already noted in other works[43,44], due to the rectangular geometry, an effect of lateral walls was found: the materials stopped with a slope profile and runout length that slightly depended on the ratio between the thickness of the box (W) and particle size (D). This is evident considering the dry coarsest particles ($W/D = 10$) for which the normalized runout length was $\sim 13\%$ lower than with the finest material ($W/D = 25$).

TABLE II. Parameters used in DEM simulations.

Solid density[a] ρ_s [kg/m^3]	Normal stiffness[b] k_n [kN/m]	Tangential stiffness[b] k_s [kN/m]	Contact friction coeff.[b] $\tan\phi_\mu$	Norm. and tang. viscous damping coeff.[c] n
2532	400	100	0.62	0.1

[a] Measured by liquid picnometry.
[b] Calibrated with triaxial tests.
[c] Estimated and then calibrated on the dry collapse tests.

V. DEM SIMULATIONS

The experimental tests were reproduced with 1:1 scale simulations with the aim of validating the numerical model and investigating the effect of different physical variables (particle size, liquid content, surface tension) on the column collapse dynamics. Numerical simulations have been also extended to conditions not studied in the laboratory such as lower solid particle density, different contact angles, different initial geometries and different lateral wall removing mechanisms. The study was focused on two particle sizes, D=2 and D=5 mm.

The granular mass was simulated using the pendular state DEM algorithm described in section III. The number of particles was fixed in order to simulate the same weight of material adopted in the experiments. This corresponded to 2250 and 37500 particles for the 5 mm and 2 mm tests respectively.

In the simulations the wall was lifted up imposing an upward acceleration equal to the gravitational acceleration, as in the laboratory tests. However, since in literature many numerical collapse tests have been carried out applying a instantaneous horizontal displacement to remove the wall, or without mention about the technique, this aspect has been specifically addressed with dedicated simulations. In particular two different wall removal mechanisms have been simulated: the instantaneous removal of the wall and the removal by uplift in vertical direction with acceleration g. Only slight differences were observed for the two cases and therefore wall removal mechanisms will not be considered further.

The surface profiles were extracted from numerical simulations considering an average profile on a internal slice 2-cm thick located on the axis of symmetry of the test device.

The DEM model required the assignation of physical and contact parameters that were calibrated on the base of dedicated laboratory experiments. The solid density of the spheres was the glass density. For the contact parameters the elastic normal and tangential stiffness (k_n and k_t) of the springs and the contact friction coefficient ($\mu = \tan\phi_\mu$) of the slider were calibrated by comparing results of triaxial tests performed with glass spheres at confinement stresses σ_3 equal to 25, 50, 100 and 200 kPa with true cubic triaxial test simulations[36]. The damping parameter was at first roughly estimated by simple restitution coefficient tests and then was finely tuned by comparing experimental and simulated final collapsed profiles of 2 mm spheres in dry conditions.

Table II lists the values of all the contact parameters used in the DEM simulations. The same parameters (stiffness, damping and friction) were applied in wet conditions and to the sphere-wall contact model.

A. Experimental vs numerical results

DEM simulations were first compared with laboratory tests focusing on the final slope profiles and run-out lengths in order to verify the behaviour of the model.

Figure 6 shows the qualitative behaviour of two simulations carried out in the dry and wet case, analogously to what was done in Figure 4 for the lab tests. A more direct comparison is presented in Figure 7 where some selected final profiles obtained for 2 mm spheres are

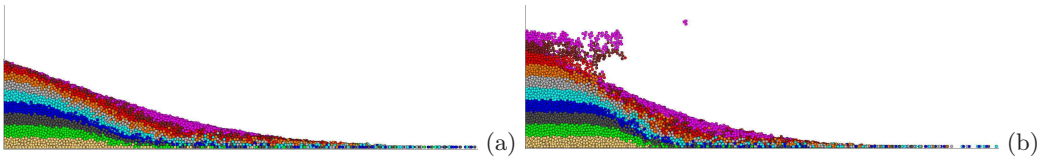

FIG. 6. Simulated final profiles for $D = 2$ mm; (a) dry; (b) $\gamma = 72.75$ mN/m (water); liquid content $w = 0.5\%$.

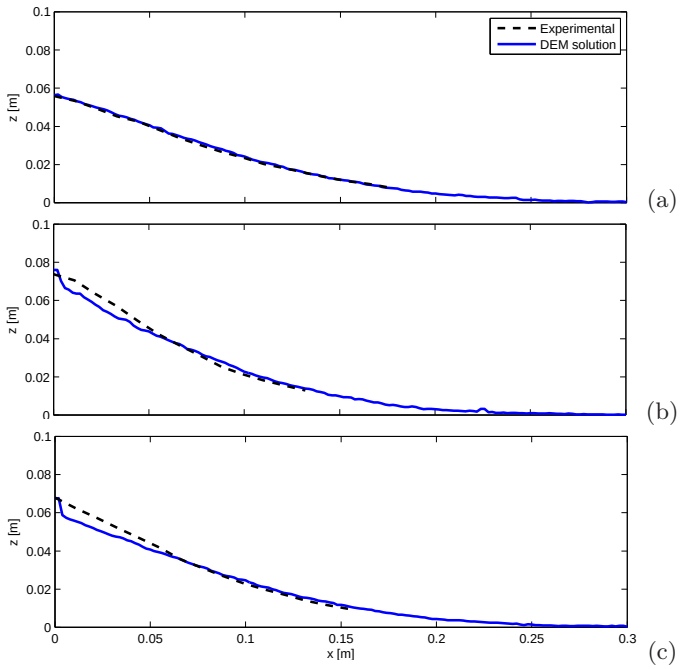

FIG. 7. Comparisons of the final profiles obtained by experimental and numerical tests for:
(a) $D = 2$ mm; $w = 0\%$ (dry);
(b) $D = 2$ mm; $w = 1\%$; $\gamma = 72.75$ mN/m (water);
(c) $D = 2$ mm; $w = 1\%$; $\gamma = 17.1$ mN/m (water+surfactant).

shown. Finally, a summary of all the comparisons between the lab and simulated tests is reported in Figures 8a,b in terms of run-out length values for different liquid contents and liquid tensions.

Since the dry test with $D = 2$mm was used for calibration it is not surprising that a good matching was found in slope profiles (see Fig. 7a) and run-out values.

Also for the wet cases the shape of the slopes fairly agree with the experiments: the final repose profiles result similar both with distilled water and adding the surfactant (see Fig. 7b,c). For these two cases small discrepancies regard the top and the toe angles which appeared slightly lower than the real ones. This reflected, more generally, on the runout lengths of all the finer particles which were systematically overestimated for all the moisture contents, both with distilled water and with water+surfactant (see Fig. 8a,b). On the contrary, for the coarsest spheres, the run-out values were better estimated for the samples mixed with water (they were inside the error bars), while they resulted different in values and trend for the low surface tension case.

A closer examination of the mechanical behaviour of the particles at the toe can provide a partial answer to the overestimation of the runout values. The simulations revealed that at the toe there were particle rotations despite of the presence of many capillary bridges. This was supposed to be unrealistic since the liquid bridge between two moving surface should oppose a rotational resistance which is closely related to the hysteretic behaviour

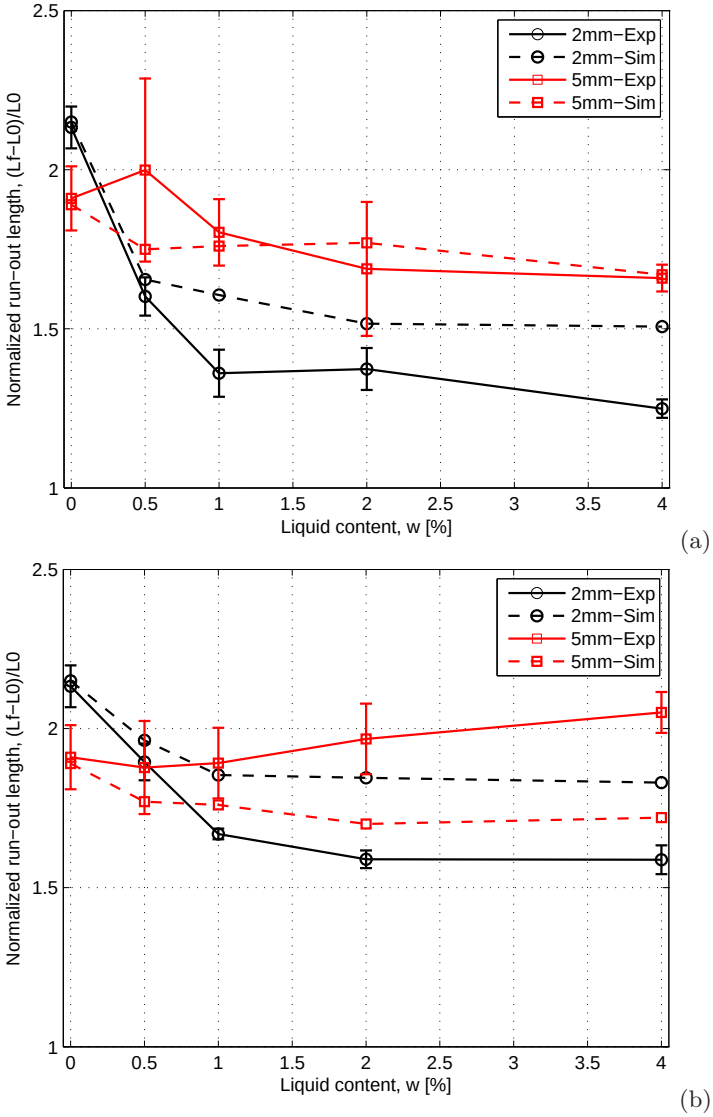

FIG. 8. Comparison of the normalized runout length from experiments (*Exp*) and DEM simulations (*Sim*) using (a) water ($\gamma = 72.75$ mN/m) and (b) water + surfactant ($\gamma = 17.1$ mN/m).

of the contact angle and the consequent energy dissipation. With respect to this aspect, a model for the rolling resistance of capillary bridges should be included in future analyses.

With regards to the discrepancies observed with the coarsest spheres in the wet case the lack of a lubrication model at the contacts may be the main reason. Lubrication force is a repulsive force that reach its maximum during collapse, lowering the frequency of frictional contacts. This is consistent with the fact that the differences regarded the coarsest spheres with the highest liquid contents and that the magnitude of the lubrication force increased with diameter and liquid volume. However, a clear and straightforward understanding of the underlying physics would require dedicated experiments and a more complex contact model which, at the time, cannot be included in this work.

Despite of these differences, we retain this model sufficient to provide important informations about the effect of the single variables of the model to the overall behaviour of the material.

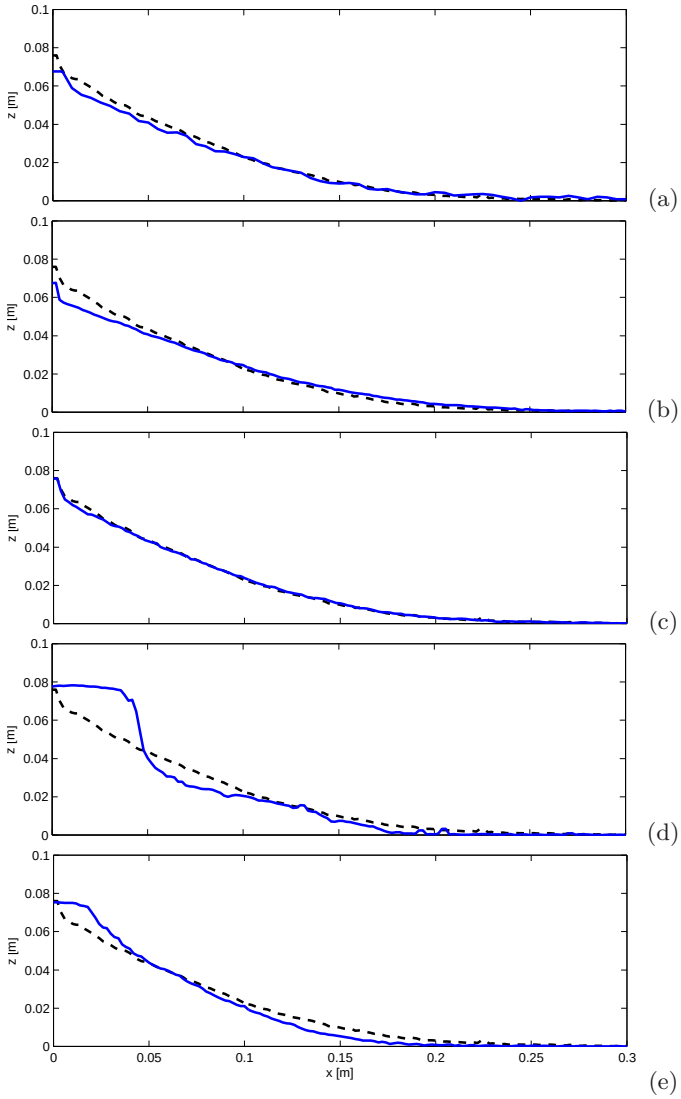

FIG. 9. Slope profile for different simulations: reference simulation (dashed line) [D = 2 mm; γ = 72.75 mN/m (water); liquid content w = 1%; contact angle $\theta = 15^o$; solid density ρ_s = 2532 kg/m^3; wall lifted with acceleration = g] vs a simulation (solid line) with:
(a) coarse particles (D = 5 mm);
(b) γ = 17.2 mN/m (water+surfactant);
(c) contact angle $\theta = 30^o$;
(d) ρ_s = 1266 kg/m^3 (half of the glass density);
(e) initial thickness W = 2.5 cm;

B. Effect of the particle size, liquid properties and solid density

In order to investigate the effect of each single variable on the final result we chose as reference case the test with the following parameters: D = 2 mm, w = 1%, γ = 72.75 mN/m, $\theta = 15^o, \rho_s$ = 2532 kg/m^3. The first group of simulations has been performed varying independently the particle size (D = 5 mm), the liquid properties (γ = 17.2 mN/m; $\theta = 30^o$) and the solid density (ρ_s = 1266 kg/m^3). The analysis of results was focused on the final profiles, that were reported in Figure 9 and compared with the reference simulation.

With the same water content but with a larger particle size (D = 5mm), the runout

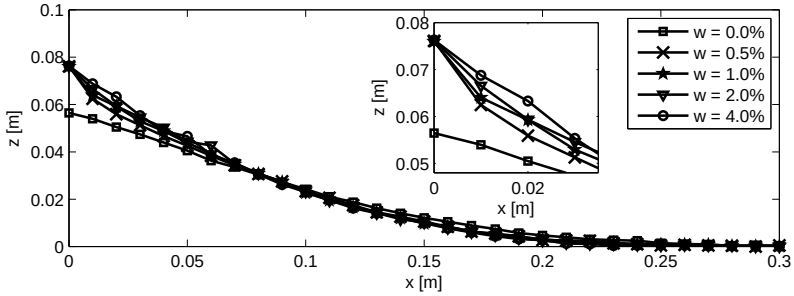

FIG. 10. Simulated final profiles for different water content w (D = 2 mm, γ = 72.75 mN/m (water)).

length resulted to be longer and the angles lower (see Fig. 9a) than in the case with finer material.

The same trends were observed with a low liquid surface tension (γ=17.1 mN/m as in the laboratory tests) (see Fig. 9b).

Instead, increasing the contact angle θ in a reasonable range (from 15 to 30^o) slightly reduced the angle at the top while the runout length and the shape at the toe remained quite unvaried (see Fig. 9c).

The scarce influence of the contact angle on the final profile may be linked to the fact that its contribution on the capillary force reduced to $\cos\theta$ and that for this hydrophilic surface its value is low, implying that $\cos\theta \approx 1$ for the different values. Furthermore, it should be noted that the contact angle value reflects on the debonding-bonding distance which decreases for larger values leading a less frequent breakage of the capillary bonds. The counterbalanced effect of these two aspects probably yields a low dependence of the profiles on the contact angle values.

On the other hand, decreasing the solid density of one half strongly modified the final profile which was then characterized by a rectangular step on the rear and a curved toe (see Fig. 9d). With regards to this test a further inspection of the dynamics of the phenomena will be reported in section V E.

C. Effect of the liquid content

In the simulations, the effect of the liquid content on the final profiles resulted similar to those observed in laboratory experiments. It can be observed considering the case with D= 2mm and distilled water by superimposing the simulated slope profiles at different moisture contents as in Figure 10: the increase of liquid content produced steeper final slope profiles. Dry and wet conditions appeared well distinct while for $w > 0$ the differences seemed slighter and concentrated at the crest of the slope. At the toe the differences can be appreciated considering the runout length plot (see Figures 8a,b): it was clear that it decreases for increasingly higher water content reaching a sort of asymptotic value. Such behaviour was observed, although in a more gentle way, also for the case with the low surface tension value (see Fig. 8b).

On the other hand, the simulations with coarse spheres (D = 5 mm) exhibited a smoother decreasing trend of the runout length with liquid content and quite constant. In this case the runout values differed from the experimental ones especially for the low liquid tension for which the experimental data indicated an opposite trend with larger runout for higher liquid content.

In literature, the presence of an asymptotic behaviour for increasingly higher water contents was also reported in the shear strength curves of unconfined radial and axial compression tests[33] and direct shear tests[45] conducted both with spheres and other granular materials. In all these tests the effect of water content seemed to saturates for w values

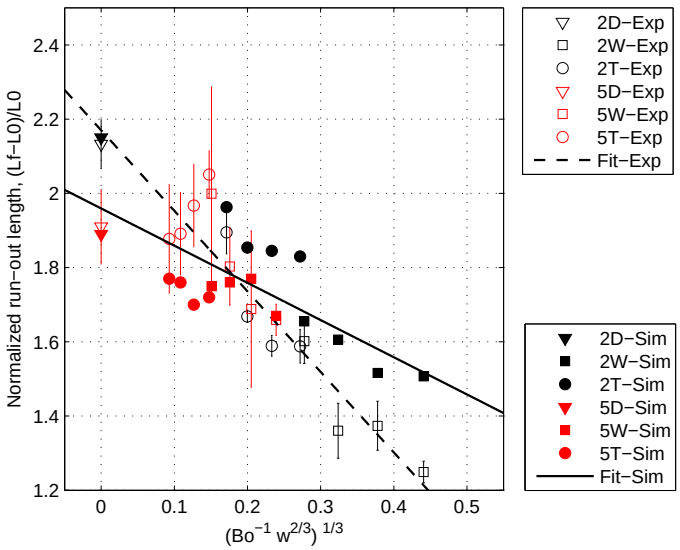

FIG. 11. Runout length vs the dimensionless number $Bo^{-1}w^{2/3}$ for the experimental (Exp) and numerical (Sim) tests. The number in the legend denotes the particle diameter, while the letter D refers to the dry case, W the case with distilled water, T the case with water and surfactant.

between 1 and 3% depending on the material used.

For a micromechanical interpretation of this behaviour we can consider a simple two-particle system. In Figure 1 the curves for capillary force vs. interparticle distance for different capillary volumes are presented. For a fixed gap the volume reduction cannot be larger than a certain value corresponding to failure of the capillary bridge. On the other hand, the volume increments slightly increase the capillary force (analytically we have $F_{cap} \propto -e^{-\sqrt{\frac{1}{V}}}$ following Soulie et al.[33] or $F_{cap} \propto -V^{-\frac{1}{2}}$ for our capillary force model[31]) and the number of potential capillary contacts (with also low capillary forces due to the larger gaps) because $s_f \propto \sqrt[3]{V}$. Furthermore, as already mentioned in section II, it can be noted that for bonds with $s = 0$ the capillary force is constant and independent of the liquid volume and failure is not theoretically possible.

Considering the macro-scale, especially if the material is dense, an increment of liquid content does not increase the number of capillary bonds in a sensible manner (and the new bridges have low capillary forces due to the large gaps) and it doesn't increase the capillary forces of those already present (which have $s = 0$ for the majority). As result, the average of the capillary forces of the packing, in comparison to the other forces, tends to a quite constant value for increasingly higher liquid content.

Again, according to the dimensional analysis on the experimental results[42], we can try to evaluate the contribution of the moisture content on the runout using a function including the Bond number, defined here as the ratio between the body and the capillary force ($Bo = \rho g R^2/\gamma$) and the liquid content w.

In Figure 11 the normalized runout values of laboratory tests and simulations were summarized in terms of a combination of Bo and w. All the data are quite well collapsed and the least square linear fitting provide a good data interpolation that confirms the adopted dimensional model. However the comparison with the fitting of the experimental data reveals the tendency for simulations to provide larger values of runout for the small diameters, and lower values for the coarse diameter and low liquid surface tension. Moreover it can be noted that the simulations of wet coarsest spheres and low liquid surface tension correlated with the liquid content while the experimental data did not, as previously commented.

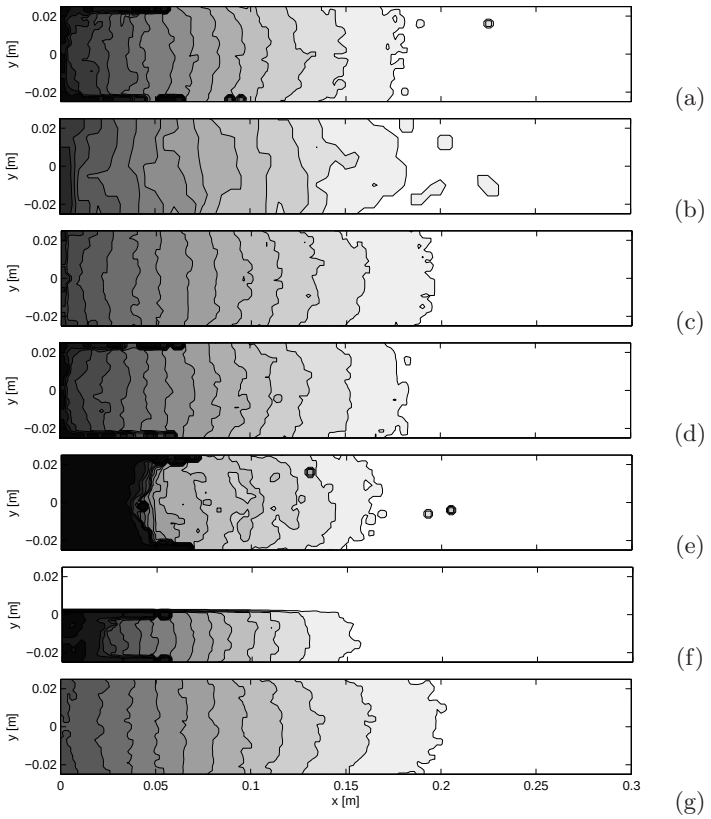

FIG. 12. Contour lines of the surface for:
(a) the reference simulation [$D = 2$ mm; $\gamma = 72.75$ mN/m (water); liquid content $w = 1\%$; contact angle $\theta = 15^o$; solid density $\rho_s = 2532\ kg/m^3$ (glass); wall lifted with acceleration $= g$]
(b) as in (a) but with coarse particles ($D = 5$ mm);
(c) as in (a) but with $\gamma = 17.2$ mN/m (water+surfactant);
(d) as in (a) but with contact angle $\theta = 30^o$;
(e) as in (a) but with $\rho_s = 1266\ kg/m^3$ (half of the glass density);
(f) as in (a) but with initial thickness $W = 2.5$ cm;
(g) as in (a) but with liquid content $w = 0\%$ (dry);

D. Effect of the boundary walls

In order to appreciate the effect of side walls on the collapse it is useful to observe the shape of the slope surface from a virtual top aerial view. Figure 12 collects several simulations results for this purpose.

The first observation is that the shape of the profiles depended on the distance from the lateral walls: the angles of the slopes were generally gentler and with a larger runout length in the middle section than near the walls. Moreover, observing the contour lines, two different zones related with different collapse mechanisms could be recognized: in the upper part of the slope the surface of the final deposit had preferentially a positive (sometimes low) concavity in transversal direction; on the other hand, at the toe of the profile the surface presented a more pronounced negative concavity.

Passing from the reference case to the case with $D = 5$mm and then to the case with a low liquid surface tension (Fig. 12a,b,c) we can observe how the retaining effect of the boundary walls tends to disappear becoming analogue to the dry case (Fig. 12g). The differences are magnified by the absence of particles glued to the lateral wall in the upper portion of the column which reveals the reduction in magnitude of the capillary force. As previously discussed, assigning $\theta = 30^o$ did not modify the final slope significantly and the

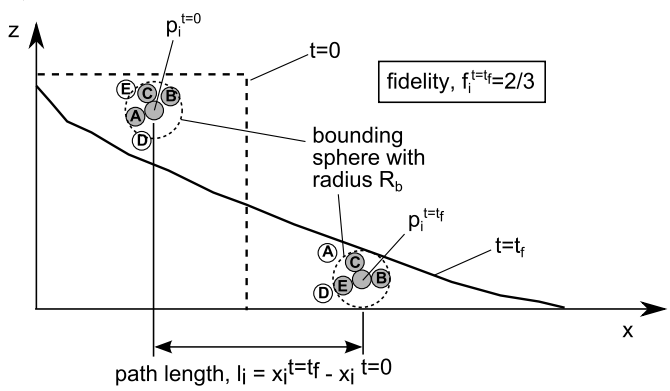

FIG. 13. Example of path-length (l_i) and fidelity (f_i) calculation for a generic particle p_i.

boundary wall effect is similar to the reference case (see Fig. 12d vs. a). On the contrary, relevant differences were observed with a low solid density (Fig. 12e vs. a): a large portion of the initial column remained stable, glued to the rear walls while only a small curved wedge detached subjected to gravity. A similar result was obtained reducing the thickness of the model of one half (from $W/D = 50$ to 25): the final slope showed a vertical narrow column constrained on the rear and a smaller portion collapsed at the toe (Fig. 12f).

All these results are consistent with the expected effect of the boundary walls: we can assume that with capillary bonds the coulombian maximum tangential forces at the contact are higher than in dry case. It means that maximum shear stress is higher. Given that the yield stress is generally higher in wet conditions, the incipient movement of the mass (for low shear rate, at the top of the column) will be favoured in dry than in wet conditions, while for larger shear rate (in the fully-developed phase of the collapse, at the toe) the two rheologies tend to be similar. This effect is larger in the upper part and lower at the toe where inertial forces prevail and a flow regime quite close to the collisional one produces frequent capillary debonding events. The solid density affects the normal and tangential stresses experienced by particle-particle and particle-wall contacts: the lower the density, the lower the mobilized stresses and the chance of local failures.

The stronger effect of the wall-particles meniscus than of the particle-particle meniscus can be explained by computing the capillary force magnitude for such cases. Following the same assumptions as in the in Appendix (relative to the sphere-sphere contact) and assuming a gap $s = 0$, the capillary force between a sphere and a flat surface becomes twice the capillary force between two equal particles. This explains the higher probability to have particles "glued" to the lateral walls and the fact that the weakest failure plane tends to move inwards further modifying the velocity profile in transversal direction. From a qualitative point of view, for 2 mm spheres, numerical simulations predict that some triplets of particles may remain stick to the walls; similar structures were not present for coarser particles. The same phenomenon was observed in the experiments, where 2 mm spheres were found to form triplets in contact with the wall, while 3 and 5 mm ones did not.

E. Analysis of the paths and of the bond durability

The dynamics of the collapse is usually deduced from the slope profiles in terms of velocity of the front and evolution of the shape, or from lateral views that allow the measurement of the velocity field.

With the aim of reconstructing the history of the system in more detail, two new simple indexes able to track the motion of the particles and the "quality" of the particle-particle relationships will be introduced.

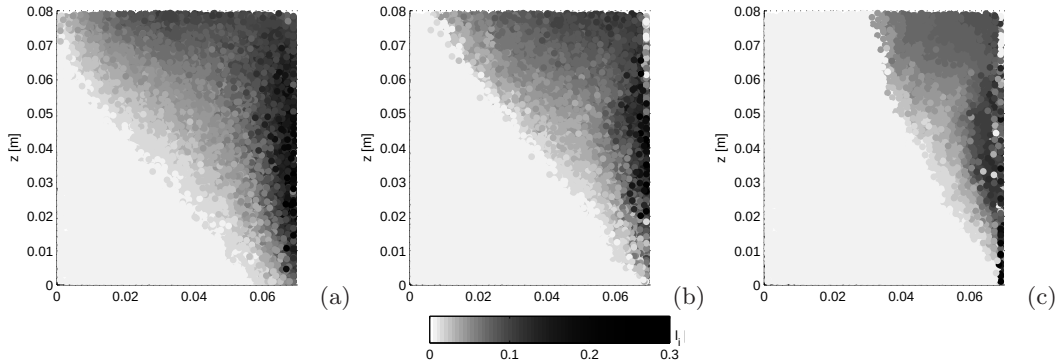

FIG. 14. Path-length values for: (a) $D = 2$ mm, dry glass sphere ($\rho_s = 2532\ kg/m^3$); (b) $D = 2$ mm, wet glass sphere ($\gamma = 72.75$ mN/m, $w = 1\%$, $\rho_s = 2532\ kg/m^3$); (c) $D = 2$ mm, wet sphere half solid density of glass ($\gamma = 72.75$ mN/m; $w = 1\%$; $\rho_s = 1266\ kg/m^3$).

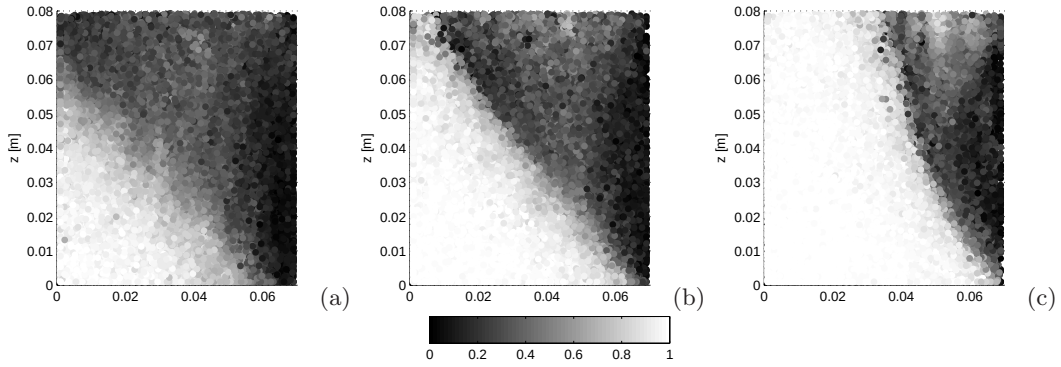

FIG. 15. Fidelity f_i of each particle for: (a) $D = 2$ mm, dry glass sphere ($\rho_s = 2532\ kg/m^3$); (b) $D = 2$ mm, wet glass sphere ($\gamma = 72.75$ mN/m, $w = 1\%$, $\rho_s = 2532\ kg/m^3$); (c) $D = 2$ mm, wet sphere half solid density of glass ($\gamma = 72.75$ mN/m; $w = 1\%$; $\rho_s = 1266\ kg/m^3$).

Firstly, let's consider the final particle positions with respect to the initial ones. As sketched in Figure 13, we defined the path-length l_i along x-axis as the x-distance between the final and the initial position of each particle; this measure helps us to recognize the static zones, the distribution of mobility of the mass in the runout direction and zones with affine motion.

Figures 14a-c depict the path-length of particles in a middle section 1-cm thick, plotted with respect to the initial particle position. Generally, particles near the movable wall at a middle-low height (in the darkest region) experience the larger path-length with respect to the others, since they are squeezed (compression for overburdened and not confined stress) and projected along x-direction[17]. During their motion the behaviour is almost collisional. Differently, on the upper part of the column the motion is more ordered and similar to a "pure shear". This can be argued noting the path-length value distribution: larger at the surface of the column with a regular decrease with depth and a little clockwise rotation of the gradient due to the progressive evolution of the slope surface.

In particular Figure 14a-c displays 3 cases with $D = 2mm$: dry, wet and half density. The globally mobilized wedge (with $l_i > 0$) is very different in the three cases while the "squeezed zone" is not so much. In the dry case the wedge touches the rear wall while in the other two cases it does not, meaning that the mobilized zone was reduced. Moreover the sliding surface became steep and curved especially in the half density wet case. It is also evident that the half density case presented a quite rigid wedge at the surface, represented by a quite constant value of the path-length.

In order to combine particle proximity information with the durability of neighbouring relationships, let's now define the particle fidelity coefficient f_i: for each particle we identify the near "fiducial particles" as the spheres that are inside a bounding spherical region of radius R_b, centred on the considered particle, in the initial state and in the final stage (after the collapse). The ratio between the number of neighbouring particles (inside the bounding sphere) in the initial state over the number of the identical particles in the final condition was defined "fidelity" An example of fidelity calculation was reported in Figure 13. By definition this number spans from zero to one: it is equal to 1 if all the neighbour particles at the beginning are the same in the final state and zero otherwise.

It should be stated that particle fidelity depends on strain level with the advantage that is not sensitive to rotations. If convection phenomena are present the particle fidelity can have localized maxima (clustered particles).

As a consequence, higher fidelity values may be expected in wet than in dry case: during shear, couples of particles connected by capillary bonds with larger attractive forces remain in touch if the disturbance is not very high.

Again, Figure 15a-c displays 3 cases: dry, wet and half density. As expected, comparing Figure 15a and b it is evident that higher fidelity zones are more frequent in the wet than in the dry case. Especially in the wet conditions, minimum values of fidelity localize in a narrow surface that coincides with the failure surface predicted by the path-length distribution and the triangle over this surface seems to move rigidly. Instead, in the dry case the failure surface was not so clearly defined since every particles moved independently. The half solid density case (Fig. 15c) provided a further reduction of the mobilized zone and increased the frequency of high fidelity values. This supported the observation that in the wet case, especially for low solid density, the motion of the unstable wedge was quite rigid while frequent bond breakages were experienced by the particles in the shear plane, between the stable portion of the column and the rigid wedge.

VI. CONCLUSIONS

A micromechanical model for granular materials in the pendular state was defined. It incorporated a capillary force model that derived from the minimum energy approach, a physical law for the bonding-debonding mechanism and a model that stored the little droplet on the surface of the particles and that followed their motion.

Discrete Element simulations of column collapse tests were successfully performed to mimic 1:1 scale experiments on wet and dry spheres. The comparison resulted qualitatively good for different diameters and liquid tension. The general trends was well captured and the important effect of the presence of liquid was observed: wet conditions presented steeper final profiles while the reduction of the liquid tension or the increase in particle diameter tended to reduce this effect. All these aspects can be explained in terms of the ratio between body and capillary forces (i.e. Bond number). The estimation of the profiles, particularly at the toe of the slopes, was not completely successful: many particles at the base were free to rolls despite of the existence of a ball-wall liquid bridge. This fact overestimated the runout distance of wet spheres and it was ascribed to the lack of a rolling resistance for the capillary bonds. On the contrary, for the big spheres, runout values resulted underestimated and the behaviour is compatible with the lack of a lubrication force at the contact.

Collapse simulations in wet conditions highlighted that, from a micromechanical standpoint, the final slope can be divided into three different zones: the static zone (under the failure plane), the upper part, near the rear wall, and the toe of the slope. The top of the slope experienced "quasi-static" phenomena that highlighted the capillary force effects between particles and between particles and lateral walls. Conversely, at the toe, the dynamics was ruled by unbalanced forces that destroyed the capillary bonds minimizing their effect.

As consequence, greater differences between wet and dry states were observed in the rear of the slope where low shear rates prevailed in almost all the test duration. On the other

hand, at the toe of the slope, the repose profiles were not so different for different liquid contents. Furthermore, in agreement with experiments, considering larger particle size, the capillary forces increased lower than the body forces. This explained why, in simulations and laboratory experiments, the larger the particle radius the lower the distance between wet and dry profiles.

Many variables influenced the final profile of the wet material: a part from the moisture content and particle size, some of them can be linked to the finite size effect (the thickness of the channel with respect to the grain size), others to the ratio between inertial and capillary forces (liquid tension, contact angle, solid density).

Other variables instead showed very small effects: the liquid-solid contact angle (in a reasonable range of values) and the mechanism of wall removal seemed not influential. Using virtual conditions like the half solid density case was useful to predict the collapse mechanism at different gravities and to appreciate different ratios between capillary and body forces.

In order to recognize the internal mechanism of collapse we used a simple quantity, called path-length, that tracked each particle from its initial position to the final "destination". Following this strategy we were able to observe that particles positioned at a middle height of the column and near the movable wall reached the largest runout distance: at the first stages of the collapse they were squeezed in horizontal direction, like in a plug flow velocity field. This important aspect as well as the observation of different regimes (quasi-static and collisional) during time in different zones of the mass are some key issues that should be taken into account when passing to continuum approaches in which classically the depth-average assumption is employed.

To investigate the cohesive behaviour of the material and the possible aggregation of the particles due to capillary bonds we introduced a new particle quantity called "fidelity". The value of this variable describes the level of damage of the bonds near each particle: no clusters formed in dry conditions with exception of the static zone. In wet case, instead, fidelity revealed the presence of many pendular clusters that were concentrated on the upper part of the column where rigid-like mechanism were observed. Furthermore, low values of fidelity showed the location of the failure plane, whose angle was steeper and well defined in wet case.

The adopted model gave good qualitative results which can be further improved, also quantitatively, once the rolling resistance and contact lubrication will be incorporated. In order to complete the understanding of the collapse in partial saturation conditions, the effects of initial capillary distribution and of higher water content (funicular state) need to be addressed in the future.

Appendix A: The capillary force

The total energy to be spent to form a liquid bridge between two equal spheres is equal to the difference between the energy required to form the solid-liquid interface and that lost at the solid-air interface[46]:

$$\begin{aligned} W_{tot} &= 2\pi\gamma R s \sin\beta + 2\pi\gamma R \sin^3\beta \\ &+2\pi\gamma_{sl} R^2 \sin^2\beta - 2\pi\gamma_{sv} R^2 \sin^2\beta \end{aligned} \tag{A1}$$

where γ_{sl} and γ_{sv} are the solid-air and solid-liquid interfacial tension.

For small s and β, and considering the validity of the Young-Dupre equation ($\gamma\cos\theta = \gamma_{sv} - \gamma_{sl}$) the Eq. A1 reduced to[28]:

$$W_{tot} = -2\pi\gamma R^2\beta^2\cos\theta \tag{A2}$$

The attractive force results as:

$$F_{cap} = -\frac{dW}{ds} = 4\pi R^2\beta\gamma\cos\theta\frac{d\beta}{ds} \tag{A3}$$

The meniscus volume may be represented in a cylindrical geometry by:

$$V = \pi R^2 \sin^2\beta\,(b+2s) - \left(\frac{\pi R^3}{3}\right)\left(1 - cos\beta^2\right)(2 + cos\beta) \tag{A4}$$

assuming small β and the wet profile of the sphere as a parabola ($b \approx R\beta^2/2$) the liquid volume becomes[30]:

$$V = \pi R^2 \beta^2 s + \frac{1}{2}\pi R^3 \beta^4 \tag{A5}$$

Assuming the invariance of the liquid bridge volume with the inter-particle distance ($dV/ds = 0$), one obtains:

$$\frac{d\beta}{ds} = -\frac{1}{(2s/\beta) + 2R\beta} \tag{A6}$$

and finally:

$$F_{cap}(s,V) = -\frac{2\pi R\gamma\cos\theta}{1 + [s/2b(s,V)]} \tag{A7}$$

where $b(s,V)$ represents the wet spherical segment on particle surface (Fig. 2), defined as:

$$b(s,V) = (s/2)\left[-1 + \sqrt{1 + 2V/(\pi R s^2)}\right] \tag{A8}$$

Appendix B: The capillary rupture and formation

This part of the algorithm manages capillary bridge rupture, redistribution and formation which are expected for large deformation of the wet granular material. These mechanisms are sketched in Figure 16 for clarity.

When two particles reached the rupture distance s_f the liquid was splitted into two equal volume drops and assigned to the two particles while the originary capillary volume of that specific potential contact was set to zero. The effect of gravity on the redistribution was neglected.

At each time-step a simple liquid drop kinematics on the particle surface was considered: the motion of each drop was associated to the motion (displacement and rotation) of the relative particle at which it was attached neglecting the variation of the particle centre of mass.

The capillary bridge formation was ruled as in the following: two single drops of volume V_1 and V_2, were assumed to lay on the surface of two different particles of radius R with two different "direction" $\boldsymbol{u_1}$ and $\boldsymbol{u_2}$ (see Fig. 16b,c). β_1 and β_2 were the two positive "filling angles" of the drops (that in general are different from the "filling angles" of the capillary bridges). The normalized vector joining the center of particle i with particle j was $\hat{\boldsymbol{d}}^{\boldsymbol{ij}}$. When the two particles approached, the formation of a new liquid bridge could happen only if $\|\boldsymbol{d}^{\boldsymbol{ij}}\| - 2R \leq s_c$. As second step, the "directions" of the two drops $\boldsymbol{u_1}$ and $\boldsymbol{u_2}$ and their filling angles β_1 and β_2 were checked with respect to the unit vector $\hat{\boldsymbol{d}}^{\boldsymbol{ij}}$ leading to three possibilities: no formation of capillary volumes; the formation of one bridge of volume $V = V_1$ (or $V = V_2$) from a single drop (see Fig. 16b); the formation of one bridge of volume $V = V_1 + V_2$ when the two drops coalesced (see Fig. 16c).

The angles β_1 and β_2 should be related to the volume of the sessile drops, the particle radius and the value of the contact angles. However, for the sake of simplicity, it was assumed a fixed drop-filling angle $\psi = \beta_1 = \beta_2 = 45^o$ as a constant in the model.

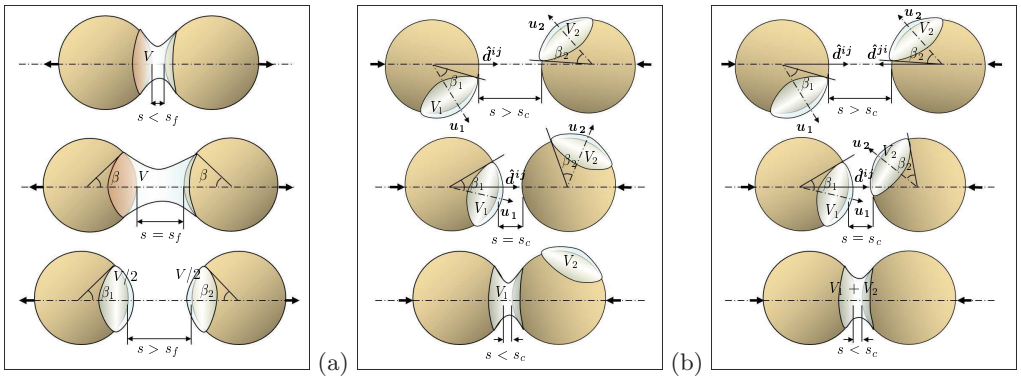

FIG. 16. (a) Failure and (b) formation of a capillary bridge from a single drop and (c) from two drops.

[1] D. J. Hornbaker, R. Albert, I. Albert, A.-L. Barabasi, and P. Schiffer, Nature **387**, 765 (1997).
[2] A. Kudrolli, Nature Materials **7**, 174 (2008).
[3] S. Nowak, A. Samadani, and A. Kudrolli, Nat Phys **1**, 50 (2005).
[4] M. Pakpour, M. Habibi, P. Mller, and D. Bonn, Sci. Rep. **2** (2012).
[5] D. M. Newitt and J. M. Conway-Jones, Trans. Inst. Chem. Eng. **36**, 422 (1958).
[6] S. Ouaguenouni and J.-N. Roux, Europhys. Lett. **32**, 449 (1995).
[7] O. Pitois, P. Moucheront, and X. Chateau, Journal of Colloid and Interface Science **231**, 26 (2000).
[8] J. C. Martin and W. J. Moyce, Philosophical Transactions of the Royal Society of London. Series A, Mathematical and Physical Sciences **244**, pp. 312 (1952), ISSN 00804614.
[9] G. Lube, H. E. Huppert, Sparks, and M. A. Hallworth, Journal of Fluid Mechanics **508**, 175 (2004).
[10] E. Lajeunesse, Mangeney-Castelnau, and J. A., Vilotte, Physics of Fluids **16**, 2371 (2004).
[11] G. Lube, H. Huppert, R. Sparks, and A. Freundt, Physical Review E - Statistical, Nonlinear, and Soft Matter Physics **72**, 1 (2005).
[12] S. Siavoshi, A. V. Orpe, and A. Kudrolli (2005), phys. Rev. E (rapid communication); e-print: cond-mat/0512575.
[13] E. Lajeunesse, J. Monnier, and G. Homsy, Physics of Fluids **17** (2005).
[14] N. Balmforth and R. Kerswell, Journal of Fluid Mechanics **538**, 399 (2005).
[15] L. Rondon, O. Pouliquen, and P. Aussillous, Physics of Fluids **23**, 073301 (pages 7) (2011).
[16] V. Topin, Y. Monerie, F. Perales, and F. Radjaï, Phys. Rev. Lett. **109**, 188001 (2012).
[17] L. Staron and E. J. Hinch, Journal of Fluid Mechanics **545**, 1 (2005).
[18] E. Larrieu, L. Staron, and E. Hinch, Journal of Fluid Mechanics **554**, 259 (2006).
[19] L. Lacaze and R. R. Kerswell, Phys. Rev. Lett. **102**, 108305 (2009).
[20] P.-Y. Lagre, L. Staron, and S. Popinet, Journal of Fluid Mechanics **686**, 378 (2011), ISSN 1469-7645.
[21] L. Girolami, V. Hergault, G. Vinay, and A. Wachs, Granular Matter pp. 1–12 (2012), ISSN 1434-5021.
[22] S. B. Savage and K. Hutter, J. Fluid Mech. **199**, 177 (1989).
[23] B. Pitman, C. Nichita, A. Patra, A. Bauer, M. Sheridan, and M. Bursik, Physics of Fluids **15**, 3638 (2003).
[24] R. Kerswell, Physics of Fluids **17**, 1 (2005).
[25] E. Doyle, H. Huppert, G. Lube, H. Mader, and R. Sparks, Physics of Fluids **19** (2007).
[26] G. B. Crosta, S. Imposimato, and D. Roddeman, Journal of Geophysical Research: Earth Surface **114**, n/a (2009), ISSN 2156-2202.
[27] G. Lian, C. Thornton, and M. Adams, Journal of Colloid and Interface Science **161**, 138 (1993).
[28] J. N. Israelachvili, *Intermolecular and surface forces / Jacob N. Israelachvili* (Academic Press, London ; San Diego :, 1991), 2nd ed., ISBN 0123751810.
[29] C. D. Willett, S. A. Johnson, M. J. Adams, and J. P. Seville, in *Granulation*, edited by M. H. A.D. Salman and J. Seville (Elsevier Science B.V., 2007), vol. 11 of *Handbook of Powder Technology*, pp. 1317 – 1351.
[30] Y. I. Rabinovich, M. S. Esayanur, and B. M. Moudgil, Langmuir **21**, 10992 (2005), http://pubs.acs.org/doi/pdf/10.1021/la0517639.
[31] P. Lambert, A. Chau, A. Delchambre, and S. Regnier, Langmuir **24**, 3157 (2008), http://pubs.acs.org/doi/pdf/10.1021/la7036444.
[32] R. A. Fisher, J. Agricult. Sci. **16**, 492 (1926).
[33] F. Soulié, F. Cherblanc, M. El Youssoufi, and C. Saix, International Journal for Numerical and Analytical Methods in Geomechanics **30**, 213 (2006), ISSN 1096-9853.
[34] V. Richefeu, M. S. El Youssoufi, R. Peyroux, and F. Radjaï, International Journal for Numerical and Analytical Methods in Geomechanics **32**, 1365 (2008), ISSN 1096-9853.
[35] C. D. Willett, M. J. Adams, S. A. Johnson, and J. P. K. Seville, Langmuir **16**, 9396 (2000), http://pubs.acs.org/doi/pdf/10.1021/la000657y.

[36]F. Gabrieli, P. Lambert, S. Cola, and F. Calvetti, International Journal for Numerical and Analytical Methods in Geomechanics **36**, 918 (2012), ISSN 1096-9853.
[37]A. Faghri, Yuwen Zhang, Numerical Heat Transfer, Part A: Applications **39**, 227 (2001), http://www.tandfonline.com/doi/pdf/10.1080/104077801300006562.
[38]E. Shahraeeni and D. Or, Phys. Rev. E **85**, 016317 (2012).
[39]P. A. Cundall and O. D. L. Strack, Géotechnique **29**, 47 (1979).
[40]L. Scholtes, P.-Y. Hicher, F. Nicot, B. Chareyre, and F. Darve, International Journal for Numerical and Analytical Methods in Geomechanics **33**, 1289 (2009), ISSN 1096-9853.
[41]R. Artoni, F. Gabrieli, A. Santomaso, and S. Cola, in *Discrete Element Modelling of Particulate Media* (The Royal Society of Chemistry, 2012), pp. 95–102, ISBN 978-1-84973-360-1.
[42]R. Artoni, A. C. Santomaso, F. Gabrieli, D. Tono, and S. Cola, Phys. Rev. E **87**, 032205 (2013).
[43]S. Siavoshi and A. Kudrolli, Physical Review E - Statistical, Nonlinear, and Soft Matter Physics **71**, 1 (2005).
[44]H.-T. Chou and C.-F. Lee, Granular Matter **13**, 39 (2011), ISSN 1434-5021.
[45]V. Richefeu, M. S. El Youssoufi, and F. Radjaï, Phys. Rev. E **73**, 051304 (2006).
[46]P. Lambert, Ph.D. thesis, Universit libre de Bruxelles, Belgium (2004).